Journal of Sound and Vibration (1989) 133(1), 97–123

EIGENSOLUTIONS OF JOINED/HERMETIC SHELL STRUCTURES USING THE STATE SPACE METHOD

M. S. TAVAKOLI

The George W. Woodruff School of Mechanical Engineering, Georgia Institute of Technology, Atlanta, Georgia 30332-0405, *U.S.A.*

AND

R. SINGH

Department of Mechanical Engineering, The Ohio State University, Columbus, Ohio 43210-1107, *U.S.A.*

(*Received* 3 *May* 1988, *and in revised form* 21 *September* 1988)

A substructure synthesis method based on state space mathematics is proposed for the eigensolution of axisymmetric joined/hermetic thin shell structures. In the state space method (SSM), a system of eight coupled first order differential equations is solved for each shell substructure using the Padé approximation for matrix exponentiation. The substructures are then joined by matching all of the displacement and force boundary variables. The Padé method allows a space-invariant substructure (e.g., uniform cylinder) to be treated as a continuum. Further, a space-variant substructure (e.g., cone) is assumed to be a piecewise continuum which allows one to still use the Padé method. SSM is validated by applying it to structural elements such as a cylinder, a cone, a sphere, and a toroidal segment, and comparing the predicted natural frequencies with well-known theoretical solutions. The strength of SSM from the substructure synthesis viewpoint is demonstrated by analyzing several shell structures including a hermetic capsule and a refrigeration compressor shell. In all examples, finite element method (FEM) predictions are used to support SSM results. For the compressor shell, SSM results compare well with the limited experimental data.

1. INTRODUCTION

1.1. SHELL STRUCTURE COMPLEXITIES

Structures composed of shell elements (cylinders, spheres, cones, etc.) find a wide range of application in such areas as refrigeration systems, pressure vessels, nuclear reactors, aircraft and rockets. These structures offer challenging analysis and design problems not only due to the degree of complexity of the governing shell equations, but also due to the difficulties associated with matching the boundary conditions between the substructures. Consequently, analytical solutions for such structures are inadequately investigated, and their dynamic behavior and design techniques for reduced noise and vibration are poorly understood.

In general, obtaining solutions for the vibration of a shell of revolution is not a trivial computational task. When joined shell structures are of concern, these computational difficulties are accompanied, if not overwhelmed, by the problem of proper matching of boundary conditions between the shell substructures. For instance, for a circular cylindrical shell, one would normally have to reduce and solve a large set of coupled governing equations and then enforce the continuity of at least eight variables at the junction of substructures. To get a sense of the complexity of this task, the circular cylinder of

0022-460X/89/070097+27 $03.00/0

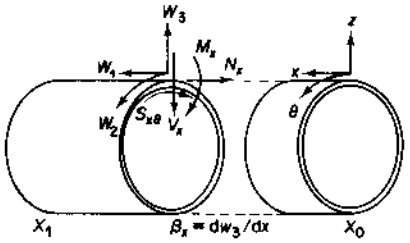

Figure 1. Circular cylindrical shell.

Figure 1 is considered. The normalized Love's equations for this cylinder are presented in equation (15) of section 3.1. The eight boundary variables shown in Figure 1 are displacements in the axial, tangential, and normal directions (W_1, W_2, W_3), slope (β_x), bending moment resultant (M_x), axial force resultant (N_x), and two Kirchhoff shear force resultants (V_x, $S_{x\theta}$). The governing equations need to be reduced in terms of these independent variables, and their matching should be enforced at the junction of substructures. Of course, one may reduce the degree of complexity by ignoring the matching of some of these variables, hence compromising the desired degree of accuracy.

1.2. LITERATURE REVIEW

None of the well-known publications on shells [1-8] deal with joined or hermetic shell structures, with the exception of the spherical shell which is a limiting case. Consequently, the closed-form solutions for classical shell geometries under classical boundary conditions have been traditionally used to establish rough guidelines for the dynamic analysis of complex shell structures [9-11]. The classical bending theory of shells was used by Kalnins [12] to analyze a paraboloidal shell of revolution and a sphere-cone combination. Hu and Raney [13] also used the classical bending theory to study a cone-cylinder combination. Smith and Haft [14] used the same theory along with Yu's decoupling procedure to analyze a cylinder clamped at one edge and closed at the other by a circular plate which was assumed to be radially rigid and constrained.

In general, shell structures have been analyzed by using approximate energy methods. Saunders and Paslay [15] employed Rayleigh's inextensional shell theory in conjunction with Hamilton's Principle to investigate a sphere-cone combination. Due to the nature of the assumed mode shapes, the continuity of the transverse and circumferential displacements were the only conditions enforced at the junction. Nevertheless, the agreement between their experimental and analytical results was within 5% for the first five modes of vibration. Ojalvo and Newman [16] used Lagrange's equations to analyze an axially rib-stiffened pressurized cylinder with a local mass attachment. The mode shapes of a simply supported cylinder were used as the trial mode functions. The receptance method was applied by Falkner [17] to a ring-stiffened cylinder closed at its ends by circular plates. The receptances for the cylinder were obtained by applying edge bending moments and transverse shear forces. Though they did not agree closely, the analytical results seemed to set the same trend as the experimental ones. Soedel [7] also employed the receptance method to study the effects of a ring attached to a simply supported cylinder.

Hirano [18] developed a systematic approach based on the minimization of the Lagrangian of a shell structure. He applied this method to a thin "drum" which is a cylinder with circular end plates. In this approach, the relevant displacements are approximated with general beam solutions. At the junctions, the continuity of the displacements and the slope is the only requirement. Several researchers [19-31] have employed this method to a number of shell structures. But this Lagrangian method is procedurally and

numerically cumbersome even though it does provide a systematic approach, and it is yet to be experimentally supported.

Various substructure synthesis methods such as the component mode synthesis method [32-39] have been applied to a variety of structural problems, but, to our knowledge, they have not been applied to the joined shell structures specifically. More recently, Irie *et al.* [40–42] used a method based on the transfer matrix approach to analyze cases such as a cone with variable thickness, and a cone-cylinder combination. Yamada [43, 44] used this method to study the vibrations of cylindrical shells with non-circular cross-sections, and also a cylindrical double shell system closed by annular end plates. This method shows a good degree of versatility and ease of application. The scope of the method is limited to structures with two and only two independent boundaries. However, this method has been applied [45-47] to unsymmetrically joined structures with more than two boundaries using branching techniques and assuming mode shapes in one direction and spanning the structure in the other direction.

Finally, it is also appropriate to mention the application of the finite element method (FEM) to shell structures. Even though this method has proven to be a powerful and at times the only applicable method for complex structures, by no means should it become a substitute for more efficient and compact analytical methods which could evolve from any of the previously mentioned methodologies. Nevertheless, FEM will be used in this work to support the analytical results.

1.3. OBJECTIVES

Motivated by recent research in this field [40-47], a substructure synthesis method based on the state space mathematics is proposed for application to joined/hermetic shell structures. The state space method (SSM) has strengths such as distributed parameter modeling, systematic, building-block fashion substructuring, exact and comprehensive matching of all boundary variables at the junctions of substructures, and the capability to model the dynamics of various axisymmetric thin shell structures easily and accurately.

In this paper, the application of SSM to structural dynamics is presented in a general fashion, and guidelines governing joining substructures with consistent as well as inconsistent coordinate systems are developed. The solution phase of the method is improved upon by adopting the Padé approximation for matrix exponentiation [48]. SSM is validated extensively by applying it to various structural elements. The results are compared to well-known theoretical results, and they are also supported by finite element method (FEM) predictions using the commercially available finite element software ANSYS [49]. Finally, the strength of SSM in substructure synthesis is demonstrated by applying it to various shell structures composed of cylindrical, conical, spherical and toroidal shells. One of these structures is an actual refrigeration compressor shell for which modal data are measured and compared with SSM results. All other SSM results are supported by FEM.

2. METHODOLOGY

2.1. STATE SPACE FORMULATION

The first step in application of the state space method (SSM) to free vibrations of an undamped continuous substructure is to collect and algebraically manipulate all of its governing equations into the form of a system of first order ordinary differential equations:

$$\{\Phi(x)\}' - [U]\{\Phi(x)\} = 0, \tag{1}$$

where x is the co-ordinate that spans the substructure from one boundary to the other,

$\{\Phi(x)\}$ represents the state vector whose elements are the relevant variables at the x boundary, $(\ )'$ indicates first derivative with respect to x, and $[U]$ is the substructure coefficient matrix containing information about its geometry, material properties, and frequency of vibration ω (a list of nomenclature is given in the Appendix).

2.2. SOLUTION PROCEDURE

The next step following the assemblage of the governing equations is to find the solution to the system of first order differential equations (1). Depending on the behavior of the coefficient matrix $[U]$, two situations may arise as follows.

2.2.1. *Space-invariant substructures*

If for a substructure, none of the elements of the coefficient matrix $[U]$ depends on the location x along the substructure, that substructure is called space-invariant. An example of such a substructure is a beam which is uniform in both its geometry and material properties. For such a substructure, the solution of equation (1) is simply:

$$\{\Phi(x)\} = \left[\exp\left(\int_x [U]\,\mathrm{d}\tau\right)\right]\{\Phi(x_0)\}. \tag{2}$$

This solution shows how the state vector at an arbitrary x can be related to the state vector at the boundary x_0 via the transfer matrix $[T(x_0, x)]$ between these two points, where

$$[T(x_0, x)] = [\exp([U](x - x_0))]. \tag{3}$$

Numerous exact and approximate methods on matrix exponentiation are available [50–52]. With ordinary matrices, these methods are more or less equivalent. However, in most structural dynamics problems, the coefficient matrix $[U]$ is ill-conditioned as a large norm and mismatch of coefficients are witnessed. Hence, most of the exponentiation methods become numerically unstable and susceptible to round-off errors. The exponentiation method proposed here is based on the eighth order Padé approximation [48] inspired by its usage in the commercially available software CTRL-C [53]. In conjunction with a quadruple precision computer, the Padé method helps to reduce the numerical limitations inherent to transfer matrix based methods.

2.2.2. *Space-variant substructures*

If for a substructure, any of the elements of the coefficient matrix $[U]$ depends on the location x along the substructure, that substructure is called space-variant. An example of this case is a tapered beam. Under such a condition, the solution to equation (1) is no longer given by equation (2) except for the rare case where $[U]$ is commutative. Hence, one needs to numerically integrate equation (1), and the solution procedure should be sought amongst the numerical integration algorithms. The Runge–Kutta method seems to have been commonly used for this case [40, 42, 44, 51]. The Peano–Baker method of integration [54] has also been used in the field of control theory. However, in order to still be able to employ the convenient Padé method, it is proposed to numerically discretize the substructure over the domain x_0 to x into intervals of size h. Then, over each step, it is assumed that equation (2) would still hold true as the solution to equations (1). Mathematically:

$$\{\Phi(x)\} = [T(x - h, x)]\{\Phi(x - h)\}, \tag{4}$$

where the transfer matrix for each step h is defined as

$$[T(x - h, x)] = \left[\exp\left(\int_{x-h}^{x} [U(\tau)]\,\mathrm{d}\tau\right)\right] \tag{5}$$

and the overall transfer matrix between x_0 and x is given by:

$$[T(x_0, x)] = [T(x-h, x)][T(x-2h, x-h)] \cdots [T(x_0, x_0+h)]. \tag{6}$$

2.3. SUBSTRUCTURE SYNTHESIS

The strength of SSM lies primarily in its ability to join substructures and match the boundary variables comprehensively. Figure 2(a) schematically shows two substructures A and B along with their individual coordinate systems to be joined along their respective common boundaries x_{1A} and x_{0B}. Here, the first subscript identifies the boundary, while the second one identifies the substructure. The state vectors at the common boundary are related through the substructure coupling matrix $[C]$ which matches the boundary variables properly according to

$$\{\Phi(x_{0B})\} = [C]\{\Phi(x_{1A})\}. \tag{7}$$

Using the global co-ordinate x_g, one can express the sate vector at any arbitrary point x_g in terms of the boundary x_{0g} as

$$\{\Phi(x_g)\} = [T(x_{0g}, x_g)]\{\Phi(x_{0g})\}, \tag{8}$$

where the transfer matrix between x_{0g} and x_g is

$$[T(x_{0g}, x_g)] = [T(x_{0A}, x_A)] \text{ for } x_{0g} \leqslant x_g \leqslant x_{1A} \text{ and } x_{0A} \leqslant x_A \leqslant x_{1A},$$
$$[T(x_{0g}, x_g)] = [T(x_{0B}, x_B)][C][T(x_{0A}, x_{1A})]$$
$$\text{for } x_{1A} \leqslant x_g \leqslant x_{1g} \text{ and } x_{0B} \leqslant x_B \leqslant x_{1B}. \tag{9}$$

In joining substructures, regardless of the orientation of the individual substructure co-ordinate systems, it is essential for the overall structure to have a global co-ordinate system which maintains its general orientation as it spans the structure from one boundary to the other. In Figure 2(a), the co-ordinate systems A and B are oriented consistent with

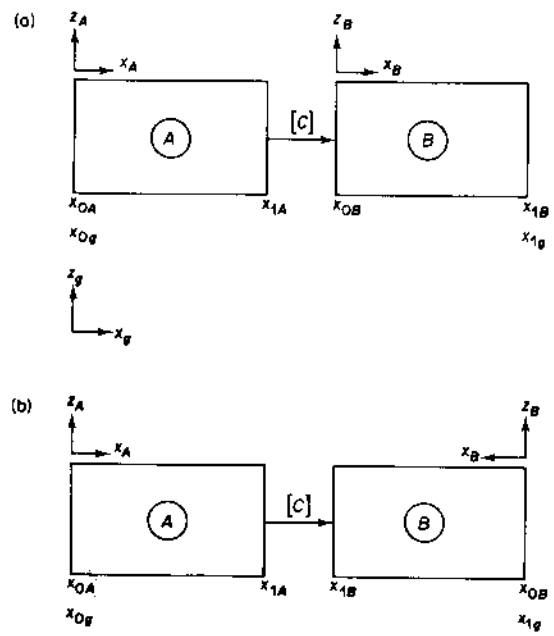

Figure 2. Synthesis of two substructures: (a) consistent substructure co-ordinates, (b) inconsistent substructure co-ordinates.

the global one. Hence, no co-ordinate adjustments are necessary. In Figure 2(b), the co-ordinate system B is oriented inconsistently with respect to the global co-ordinate system. Following a similar approach as before, one can deduce that the transfer matrix between x_{0g} and x_g for this case is

$$[T(x_{0g}, x_g)] = [T(x_{0A}, x_A)] \text{ for } x_{0g} \leqslant x_g \leqslant x_{1A} \text{ and } x_{0A} \leqslant x_A \leqslant x_{1A},$$
$$[T(x_{0g}, x_g)] = [G][T(x_B, x_{1B})]^{-1}[G]^{-1}[C][T(x_{0A}, x_{1A})]$$
$$\text{for } x_{1A} \leqslant x_g \leqslant x_{1g} \text{ and } x_{0B} \leqslant x_B \leqslant x_{1B}. \tag{10}$$

The co-ordinate transformation matrix $[G]$ is used to orient $\{\Phi(x_B)\}$ consistent with the global co-ordinate system according to

$$\{\Phi(x_g)\} = [G]\{\Phi(x_B)\} \quad \text{for} \quad x_{1A} \leqslant x_g \leqslant x_{1g} \quad \text{and} \quad x_{0B} \leqslant x_B \leqslant x_{1B}. \tag{11}$$

2.4. EIGENPROBLEM FORMULATION

Once the substructures are joined, one may use equation (8) to span the entire structure from one boundary at x_{0g} to the other at x_{1g}. At the boundaries, some of the boundary variables are zero and some are finite. Hence one can write

$$\begin{Bmatrix} \{\Phi^0(x_{1g})\} \\ \{\Phi^1(x_{1g})\} \end{Bmatrix} = \begin{bmatrix} [\tau]_{11} & [\tau]_{12} \\ [\tau]_{21} & [\tau]_{22} \end{bmatrix} \begin{Bmatrix} \{\Phi^0(x_{0g})\} \\ \{\Phi^1(x_{0g})\} \end{Bmatrix}. \tag{12}$$

Here $\{\Phi^0\}$ represents the constrained variables of the boundary vectors, and $\{\Phi^1\}$ represents the unconstrained ones. In other words, all elements of $\{\Phi^0\}$ are zero, while all elements of $\{\Phi^1\}$ are non-zero. Therefore, the eigenproblem is given by

$$[\tau]_{12}\{\Phi^1(x_{0g})\} = 0. \tag{13}$$

3. ANALYSIS OF STRUCTURAL ELEMENTS

3.1. CIRCULAR CYLINDRICAL SHELL

An axisymmetric circular cylindrical shell represents a space-invariant geometry of dimension eight. The pertinent normalized variables for this case are shown in Figure 1. The normalization is done using solutions of the type

$$(\underline{W}_1, \underline{W}_2, \underline{W}_3) = (R)(W_1 \cos(n\theta), W_2 \sin(n\theta), W_3 \cos(n\theta)),$$
$$(\underline{M}_x, \underline{M}_\theta, \underline{M}_{x\theta}) = (D/R)(M_x \cos(n\theta), M_\theta \cos(n\theta), M_{x\theta} \sin(n\theta)),$$
$$(\underline{N}_x, \underline{N}_\theta, \underline{N}_{x\theta}) = (D/R^2)(N_x \cos(n\theta), N_\theta \cos(n\theta), N_{x\theta} \sin(n\theta)),$$
$$(\underline{Q}_x, \underline{Q}_\theta) = (D/R^2)(Q_x \cos(n\theta), Q_\theta \sin(n\theta)),$$
$$(\underline{V}_x, \underline{S}_{x\theta}) = (D/R^2)(V_x \cos(n\theta), S_{x\theta} \sin(n\theta)),$$
$$\underline{\beta}_x = \beta_x \cos(n\theta), \qquad \underline{x} = (R)x, \tag{14}$$

where n is the circumferential mode number, and the unnormalized variables are underlined. The normalized Love's governing equations are [6, 7]:

$$\lambda W_1 = -N'_x - nN_x, \qquad \lambda W_2 = -N'_{x\theta} + nN_\theta - Q_\theta, \qquad \lambda W_3 = -Q'_x - nQ_\theta + N_\theta,$$
$$\beta_x = -W'_3, \qquad Q_x = M'_x + nM_{x\theta}, \qquad Q_\theta = M'_{x\theta} - nM_\theta,$$
$$V_x = Q_x + nM_{x\theta}, \qquad S_{x\theta} = N_{x\theta} + M_{x\theta}, \qquad N_x = (W'_1 + \nu(nW_2 + W_3))d,$$
$$M_x = \beta'_x + \nu(nW_2 + n^2 W_3), \qquad N_\theta = (nW_2 + W_3 + \nu W'_1)d, \qquad M_\theta = nW_2 + n^2 W_3 + \nu\beta'_x,$$
$$N_{x\theta} = (1-\nu)(W'_2 - nW_1)d/2, \qquad M_{x\theta} = (1-\nu)(W'_2 - n\beta_x). \tag{15}$$

The governing equations for this case can be arranged in the form of equation (1), where $\{\Phi(x)\}$ is given by

$$\{\Phi(x)\}^{\mathrm{T}} = \langle W_1, W_2, W_3, \beta_x, M_x, N_x, V_x, S_{x\theta} \rangle, \tag{16}$$

and the normalized non-zero elements of the coefficient matrix $[U]$ of dimension eight are:

$$U_{45} = U_{57} = -U_{34} = 1, \qquad U_{76} = -U_{13} = \nu, \qquad U_{85} = U_{86} = -U_{12} = -U_{42} = n\nu,$$
$$U_{75} = -U_{43} = n^2\nu, \qquad U_{21} = -U_{68} = nd/(2+d), \qquad U_{16} = 1/d,$$
$$U_{24} = 2n/(2+d), \qquad U_{58} = -4n/(2+d), \qquad U_{54} = -U_{51} = 2n^2d(1-\nu)/(2+d),$$
$$U_{28} = 2/(2+d)(1-\nu), \qquad U_{72} = U_{83} = n(1-\nu)(d+n^2),$$
$$U_{64} = -n^2d(1-\nu)/(2+d), \qquad U_{61} = n^2d(1-\nu)(2+d)/2 - \lambda,$$
$$U_{73} = (1-\nu^2)(d+n^4) - \lambda, \qquad U_{82} = n^2(1-\nu^2)(1+d) - \lambda. \tag{17}$$

A circular cylinder 342·9 mm long, 228·6 mm round, 2·03 mm thick, with material properties $E = 207$ GPa, $\rho = 7800$ kg/m^3, and $\nu = 0{\cdot}3$ is considered. Since both edges are shear diaphragmed

$$\{\Phi(x_0)\}^{\mathrm{T}} = \{\Phi(x_1)\}^{\mathrm{T}} = \langle W_1, 0, 0, \beta_x, 0, 0, V_x, S_{x\theta} \rangle. \tag{18}$$

Theoretical [6, 7] SSM and FEM results are given in Table 1. Except for $(n = 0, m = 0)$, SSM results are in perfect agreement with the theoretical ones. FEM results are based on a 20-element axisymmetric model with an axisymmetric conical shell element which has four degrees of freedom at each node. FEM results closely agree with theory and SSM. The theoretical model [6, 7] mispredicts the lowest torsional mode of the cylinder (at 4656 Hz) in the place of the breathing mode (at 6424 Hz). The theoretical model does predict a predominantly axial mode at 6424 Hz which is obviously incorrect.

3.2. TRUNCATED CIRCULAR CONE

An example of a space-variant geometry is the truncated circular cone shown in Figure 3 along with its pertinent variables. The dimension of this problem is eight. Using solutions

TABLE 1

Shear diaphragmed cylinder: comparison of natural frequencies in Hz

n	m	Theory	SSM	FEM [49]	Δ_1%	Δ_2%
0	*	—	4656	4656	—	—
	0	4656	6424	6424	—	—
	1	7081	7081	7085	0·0	−0·1
	2	7144	7144	7150	0·0	−0·1
1	0	2801	2801	2804	0·0	−0·1
	1	5352	5352	5359	0·0	−0·1
	2	6363	6363	6371	0·0	−0·1
2	0	1372	1372	1372	0·0	0·0
	1	3466	3466	3470	0·0	−0·1
	2	4926	4926	4933	0·0	−0·1
3	0	806	806	805	0·0	0·1
	1	2274	2274	2275	0·0	0·0
	2	3676	3676	3680	0·0	−0·1

$\Delta_1\% = 100 \times (\text{theory} - \text{SSM})/\text{theory}$.
$\Delta_1\% = 100 \times (\text{theory} - \text{FEM})/\text{theory}$.

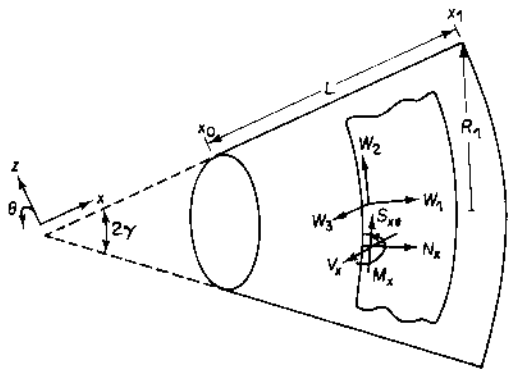

Figure 3. Circular conical shell.

of the same type as in equations (14) but replacing R with R_1, one may write the normalized governing Love's equations [6, 7] as

$$\lambda_1 W_1 = -N_x/x - nN_{x\theta}/x \sin(\gamma) + N_\theta/x - N'_x,$$

$$\lambda_1 W_2 = -N'_{x\theta} + nN_\theta/x \sin(\gamma) - 2N_{x\theta}/x - Q_\theta/x \tan(\gamma),$$

$$\lambda_1 W_3 = -Q'_x - nQ_\theta/x \sin(\gamma) - Q_x/x + N_\theta/x \tan(\gamma),$$

$$Q_x = M'_x + nM_{x\theta}/x \sin(\gamma) + M_x/x - M_\theta/x, \qquad Q_\theta = M'_{x\theta} - nM_\theta/x \sin(\gamma) + 2M_{x\theta}/x,$$

$$N_x = (W'_1 + \nu(nW_2/\sin(\gamma) + W_1 + W_3/\tan(\gamma))/x)d,$$

$$N_\theta = ((nW_2/\sin(\gamma) + W_1 + W_3/\tan(\gamma))/x + \nu W'_1)d,$$

$$N_{x\theta} = (1-\nu)(W'_2 - W_2/x - nW_1/x \sin(\gamma))d/2,$$

$$M_x = \beta'_x + \nu(-xW'_3 + n^2 W_3/\sin^2(\gamma) + nW_2/\sin(\gamma)\tan(\gamma))/x^2,$$

$$M_\theta = (-xW'_3 + n^2 W_3/\sin^2(\gamma) + nW_2/\sin(\gamma)\tan(\gamma))/x^2 + \nu\beta'_x,$$

$$M_{x\theta} = (1-\nu)(-n\beta_x/x \sin(\gamma) - nW_3/x^2 \sin(\gamma) + W'_2/x \tan(\gamma) - W_2/x^2 \tan(\gamma)),$$

$$V_x = Q_x + nM_{x\theta}/x \sin(\gamma), \qquad S_{x\theta} = N_{x\theta} + M_{x\theta}/x \tan(\gamma), \qquad \beta_x = -W'_3. \tag{19}$$

The governing equations can be arranged in the form of equation (1) where $\{\Phi(x)\}$ is given by equation (16), and the normalized non-zero elements of the coefficient matrix $[U(x)]$ of dimension eight are

$$U_{45} = U_{57} = -U_{34} = 1, \qquad U_{28} = 2x^2 \tan^2(\gamma)/\underline{d}(1-\nu),$$

$$U_{68} = -xdn \tan^2(\gamma)/\underline{d} \sin(\gamma), \qquad U_{11} = U_{44} = -\nu/x,$$

$$U_{85} = -U_{42} = n\nu/x^2 \sin(\gamma)\tan(\gamma), \qquad U_{75} = -U_{43} = n^2\nu/x^2 \sin^2(\gamma),$$

$$U_{55} = U_{66} = -(1-\nu)/x, \qquad U_{42} = -\nu n/x^2 \sin(\gamma)\tan(\gamma),$$

$$U_{52} = n(1-\nu^2)/x^3 \sin(\gamma)\tan(\gamma), \qquad U_{88} = -2(1+\underline{d})/x\underline{d},$$

$$U_{62} = nd(1-\nu^2)/x^2 \sin(\gamma), \qquad U_{22} = -U_{77} = 1/x, \qquad U_{86} = -U_{12} = \nu n/x \sin(\gamma),$$

$$U_{58} = -4n \tan(\gamma)/\underline{d} \sin(\gamma), \qquad U_{23} = 2n \tan(\gamma)/x\underline{d} \sin(\gamma),$$

$$U_{24} = 2n \tan(\gamma)/\underline{d} \sin(\gamma), \qquad U_{78} = -4n \tan(\gamma)/x\underline{d} \sin(\gamma),$$

$$U_{21} = xnd \tan^2(\gamma)/\underline{d} \sin(\gamma), \qquad U_{64} = -n^2 d(1-\nu)\tan(\gamma)/x\underline{d} \sin^2(\gamma),$$

$$U_{76} = -U_{13} = \nu/x \tan(\gamma), \qquad U_{51} = -2n^2 d(1-\nu)\tan(\gamma)/x\underline{d}\sin^2(\gamma), \qquad U_{16} = 1/d,$$

$$U_{82} = n^2(1-\nu^2)(1+d\tan^2(\gamma))/x^2\sin^2(\gamma)\tan^2(\gamma) - \lambda_1,$$

$$U_{61} = n^2 d(1-\nu)/x^2\,\underline{d}\sin^2(\gamma) + (1-\nu^2)d/x^2 - \lambda_1,$$

$$U_{53} = U_{74} = 2n^2 d(1-\nu)\tan^2(\gamma)/x\underline{d}\sin^2(\gamma) + n^2(1-\nu^2)/x^3\sin^2(\gamma),$$

$$U_{54} = 2n^2 d(1-\nu)\tan^2(\gamma)/\underline{d}\sin^2(\gamma) + (1-\nu^2)/x^2,$$

$$U_{63} = d(1-\nu^2)/x^2\tan(\gamma) - n^2 d(1-\nu)\tan(\gamma)/x^2\underline{d}\sin^2(\gamma),$$

$$U_{71} = d(1-\nu^2)/x^2\tan(\gamma) - 2n^2 d(1-\nu)\tan(\gamma)/x^2\underline{d}\sin^2(\gamma),$$

$$U_{72} = nd(1-\nu^2)/x^2\sin(\gamma)\tan(\gamma) + n^3(1-\nu^2)/x^4\sin^3(\gamma)\tan(\gamma),$$

$$U_{81} = -nd(1-\nu)/x^2\underline{d}\sin(\gamma) + nd(1-\nu^2)/x^2\sin(\gamma),$$

$$U_{84} = nd(1-\nu)\tan(\gamma)/x\underline{d}\sin(\gamma) + n(1-\nu^2)/x^3\sin(\gamma)\tan(\gamma),$$

$$U_{73} = n^4(1-\nu^2)/x^4\sin^4(\gamma) + 2n^2 d(1-\nu)\tan^2(\gamma)/x^2\underline{d}\sin^2(\gamma) + d(1-\nu^2)/x^2\tan^2(\gamma) - \lambda_1,$$

$$U_{83} = nd(1-\nu)\tan(\gamma)/x^2\sin(\gamma) + nd(1-\nu^2)/x^2\sin(\gamma)\tan(\gamma) + n^3(1-\nu^2)/x^4\sin^3(\gamma)\tan(\gamma), \tag{20}$$

where $\lambda_1 = \rho H R_1^4\omega^2/D$ and $\underline{d} = 2 + x^2 d\tan^2(\gamma)$.

For comparison purposes, the truncated cone analyzed by Naumann [55] and by Adelman *et al.* [56] is studied here. This cone has a 60° apex angle, is 0·635 mm thick, and grows from a 76·2 mm radius to a 609·6 mm base radius ($x_0/x_1 = 0{\cdot}125$). The material properties are $E = 71$ GPa, $\rho = 2700\ \text{kg/m}^3$ and $\nu = 0{\cdot}315$. The cone is clamped at the smaller end and is free at the larger one. Hence, the boundary conditions are

$$\{\Phi(x_0)\}^{\mathrm{T}} = \langle 0, 0, 0, 0, M_x, N_x, V_x, S_{x\theta}\rangle, \qquad \{\Phi(x_1)\}^{\mathrm{T}} = \langle W_1, W_2, W_3, \beta_x, 0, 0, 0, 0\rangle. \tag{21}$$

The natural frequencies are compared to theory [56] in Table 2. The theoretical values are based on Novozhilov's shell equations and the Rayleigh–Ritz method. FEM results are based on a 20-element axisymmetric model with the same element mentioned in section 3.1. SSM results were found with a step size of $h = L/50$. The results are generally in excellent agreement with each other. However, as in the case of the cylindrical shell, the theory mistakenly predicts the first torsional mode at 253 Hz in place of the first axisymmetric bending mode at 513 Hz.

TABLE 2

Clamped–free cone: comparison of natural frequencies in Hz

n	Theory	SSM	FEM [49]	Δ_1%	Δ_2%
0	253·5	253·2	—	0·1	—
0	—	512·0	513·2	—	—
1	95·6	95·4	95·8	0·2	−0·2
2	41·8	41·6	41·9	0·5	−0·2
3	23·4	23·2	23·50	0·8	−0·4

$\Delta_1\% = 100\times(\text{theory} - \text{SSM})/\text{theory}$.
$\Delta_2\% = 100\times(\text{theory} - \text{FEM})/\text{theory}$.

The effect of the step size h on the accuracy of SSM results for the truncated cone is shown in Table 3 by observing the convergence of the $n=2$ mode onto its theoretical value $f_2=41{\cdot}8$ Hz. A step size as large as $h=L/15$ seems to produce an acceptable level of accuracy.

In order to demonstrate the numerical stability of SSM, the variation of the natural frequency of mode $n=0$ versus the decreasing ratio of x_0/x_1 is shown in Table 4. The cone has the same dimensions and material properties as given before, except that the base radius is 57·7 mm and $\nu=0{\cdot}3$. Both the inner and the outer edges of the cone are kept free. Since theoretical results for such a truncated cone are not readily obtainable, SSM results for the first axisymmetric ($n=0$) natural frequency are compared to the corresponding value for a free complete cone published in reference [6] as $f_0=7993$ Hz. FEM predicts this mode to occur at $f_0=7870$ Hz. The difference between the theory and SSM or FEM is believed to be due to the fact that the theory [6] uses Donnell–Mushtari shell equations, and it also enforces free boundary conditions at the apex which are not exactly what is used here. Based on these results, the SSM model of a cone with a small "pinhole" at the apex is considered to be a practical model of a complete cone as far as eigensolutions are concerned. However, such a model is inappropriate for computing force/moment variations near the apex of a complete cone.

TABLE 3

Clamped–free cone: effect of step size h on convergence of $n=2$ natural frequency $f_2=41{\cdot}8$ Hz

L/h	SSM	$\Delta\%$
5	38·4	8·1
10	40·5	3·1
15	41·1	1·7
20	41·3	1·2
30	41·5	0·7
50	41·6	0·5

$\Delta\% = 100\times(f_2-\text{SSM})/f_2$.

TABLE 4

Truncated cone: variation of lowest axisymmetric ($n=0$) natural frequency (Hz) *versus x_0/x_1 ratio and comparison with complete cone frequency $f_0=7993$ Hz*

x_0/x_1	SSM	$\Delta\%$
0·1	7883	1·4
0·01	7878	1·4
0·001	7879	1·4
0·0001	7879	1·4

$\Delta\% = 100\times(f_0-\text{SSM})/f_0$.

3.3. SPHERICAL SHELL

The spherical shell is an example of a space-variant structural element whose governing differential equations have complicated non-constant (transcendental) coefficients. The governing equations [6, 7] are normalized by using equations (14), and the pertinent variables are shown in Figure 4. One has

$$\lambda W_1 = -N'_x - N_x/\tan(x) - nN_{x\theta}/\sin(x) + N_\theta/\tan(x) - Q_x,$$

$$\lambda W_2 = 2N_{x\theta}/\tan(x) - N'_{x\theta} + nN_\theta/\sin(x) - Q_\theta,$$

$$\lambda W_3 = -Q'_x - nQ_\theta/\sin(x) - Q_x/\tan(x) + N_x + N_\theta,$$

$$Q_x = M'_x + nM_{x\theta}/\sin(x) + M_x/\tan(x) - M_\theta/\tan(x),$$

$$Q_\theta = M'_{x\theta} - nM_\theta/\sin(x) + 2M_{x\theta}/\tan(x),$$

$$N_x = (W'_1 + W_3 + \nu(nW_2/\sin(x) + W_1/\tan(x) + W_3))d,$$

$$N_\theta = ((nW_2/\sin(x) + W_1/\tan(x) + W_3) + \nu(W'_1 + W_3))d,$$

$$N_{x\theta} = (1-\nu)(W'_2 - W_2/\tan(x) - nW_1/\sin(x))/d/2,$$

$$M_x = \beta'_x + \nu(-W'_3/\tan(x) + n^2 W_3/\sin^2(x) + W_1/\tan(x) + nW_2/\sin(x)),$$

$$M_\theta = -W'_3/\tan(x) + n^2 W_3/\sin^2(x) + W_1/\tan(x) + nW_2/\sin(x) + \nu\beta'_x,$$

$$M_{x\theta} = (1-\nu)(-n\beta_x/\sin(x) - nW_3/\sin(x)\tan(x) + W'_2 - W_2/\tan(x)),$$

$$V_x = Q_x + nM_{x\theta}/\sin(x), \qquad S_{x\theta} = N_{x\theta} + M_{x\theta}, \qquad \beta_x = W_1 - W'_3. \tag{22}$$

The state vector $\{\Phi(x)\}$ is given by equation (16), and the normalized non-zero elements of the coefficient matrix $[U(x)]$ of dimension eight are

$$U_{31} = U_{45} = U_{57} = -U_{34} = -U_{67} = 1, \qquad U_{76} = -U_{13} = 1 + \nu,$$

$$U_{68} = (2n - nd)/(2+d)\sin(x), \qquad U_{11} = U_{44} = -\nu/\tan(x),$$

$$U_{85} = U_{86} = -U_{12} = -U_{42} = n\nu/\sin(x), \qquad U_{75} = -U_{43} = n^2\nu/\sin^2(x),$$

$$U_{55} = U_{66} = -(1-\nu)/\tan(x), \qquad U_{28} = 2/(2+d)(1-\nu),$$

$$U_{52} = U_{84} = n(1-\nu^2)/\sin(x)\tan(x), \qquad U_{88} = -2/\tan(x),$$

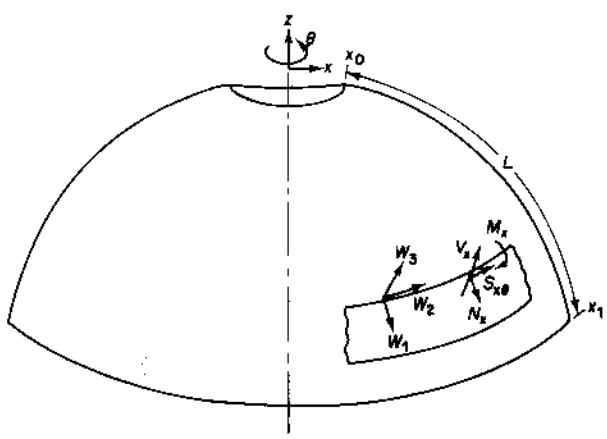

Figure 4. Spherical shell.

$$U_{62} = U_{81} = nd(1-\nu^2)/\sin(x)\tan(x), \qquad U_{22} = -U_{77} = 1/\tan(x),$$
$$U_{23} = 2n/(2+d)\sin(x)\tan(x), \qquad U_{24} = 2n/(2+d)\sin(x),$$
$$U_{78} = -4n/(2+d)\sin(x)\tan(x), \qquad U_{21} = nd/(2+d)\sin(x),$$
$$U_{54} = -U_{51} = 2n^2d(1-\nu)/(2+d)\sin^2(x), \qquad U_{58} = -4n/(2+d)\sin(x),$$
$$U_{82} = n^2(1-\nu^2)(1+d)/\sin^2(x) - \lambda, \qquad U_{64} = -2n^2d(1-\nu)/(2+d),$$
$$U_{61} = 2n^2d(1-\nu)/(2+d)\sin^2(x) + (1-\nu^2)d/\tan^2(x) - \lambda,$$
$$U_{73} = n^4(1-\nu^2)/\sin^4(x) + 2n^2d(1-\nu)/(2+d)\sin^2(x)\tan^2(x) + d(1-\nu^2) - \lambda,$$
$$U_{53} = U_{74} = 2n^2d(1-\nu)/(2+d)\sin^2(x)\tan(x) + n^2(1-\nu^2)/\sin^2(x)\tan(x),$$
$$U_{63} = U_{71} = d(1-\nu^2)/\tan(x) - 2n^2d(1-\nu)/(2+d)\sin^2(x)\tan(x),$$
$$U_{72} = U_{83} = nd(1-\nu^2)/\sin(x) + n^3(1-\nu^2)/\sin^3(x), \qquad U_{16} = 1/d. \tag{23}$$

SSM is applied to a full sphere 114·3 mm in radius, 5·7 mm in thickness, with material properties $E = 207$ GPa, $\rho = 7800$ kg/m^3 and $\nu = 0{\cdot}3$. The full sphere can be modeled by allowing $x_0 = 0{\cdot}1°$, $x_1 = 179{\cdot}9°$, and enforcing free boundary conditions at $\{\Phi(x_1)\}$ and $\{\Phi(x_0)\}$. The results are shown in Table 5. FEM results are based on a 40-element axisymmetric model, while the SSM results are for a step size of $h = L/50$. The theoretical values are extracted from reference [4]. It should be noted that the asymmetric frequencies are very close to the corresponding axisymmetric ones which is in accordance with the eigenvalue degeneracy characteristic of a full sphere [57]. Also, $(n+m)$ is always equal to the number of nodal circles on the sphere. Once again, it should be mentioned that this model is inappropriate for generating force/moment variations near the pinhole at the apex.

3.4. TOROIDAL SHELL

The governing equations of motion for the toroidal shell shown in Figure 5 are derived by incorporating the following radii of curvature in the equations of a general shell of revolution [7]:

$$R_x = R, \qquad R_\theta = R + R_0/\sin(x). \tag{24}$$

TABLE 5

Full sphere: comparison of natural frequencies in Hz

n	m	Theory	SSM	FEM [49]	Δ_1%	Δ_2%
0	2	5281	5291	5283	−0·2	0·0
	3	6321	6330	6319	−0·1	0·0
	4	6883	6894	6876	−0·1	0·1
1	1	5281	5293	5281	−0·2	0·0
	2	6321	6349	6314	−0·4	0·1
	3	6883	6944	6867	−0·9	0·2
2	0	5281	5285	5285	−0·1	−0·1
	1	6321	6323	6318	0·0	0·0
	2	6883	6886	6871	0·0	0·2
3	0	6321	6320	6324	0·0	0·0
	1	6883	6879	6876	0·0	0·1

$\Delta_1\% = 100 \times (\text{theory} - \text{SSM})/\text{theory}$.
$\Delta_2\% = 100 \times (\text{theory} - \text{FEM})/\text{theory}$.

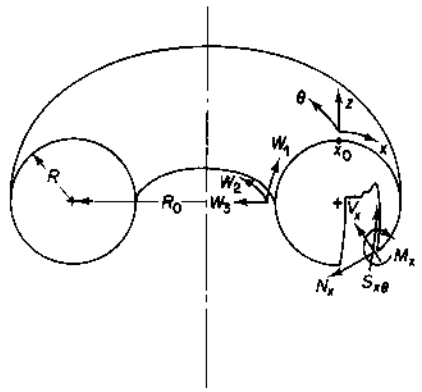

Figure 5. Toroidal shell.

Upon using these radii and the normalization equations given in equations (14), the normalized governing equations for the toroidal shell become

$$\lambda W_1 = -N'_x - b\cos(x)N_x - nbN_{x\theta} + b\cos(x)N_\theta - Q_x,$$

$$\lambda W_2 = -2b\cos(x)N_{x\theta} - N'_{x\theta} + nbN_\theta - b\sin(x)Q_\theta,$$

$$\lambda W_3 = -Q'_x - nbQ_\theta - b\cos(x)Q_x + N_x + b\sin(x)N_\theta,$$

$$Q_x = M'_x + nbM_{x\theta} + b\cos(x)M_x - b\cos(x)M_\theta, \qquad Q_\theta = M'_{x\theta} - nbM_\theta + 2b\cos(x)M_{x\theta},$$

$$N_x = (W'_1 + W_3 + \nu b(nW_2 + \cos(x)W_1 + \sin(x)W_3))d,$$

$$N_\theta = (b(nW_2 + \cos(x)W_1 + \sin(x)W_3) + \nu(W'_1 + W_3))d,$$

$$N_{x\theta} = (1-\nu)(W'_2 - b\cos(x)W_2 - nbW_1)d/2,$$

$$M_x = \beta'_x + \nu b(-\cos(x)W'_3 + n^2bW_3 + \cos(x)W_1 + nb\sin(x)W_2),$$

$$M_\theta = b(-\cos(x)W'_3 + n^2bW_3 + \cos(x)W_1 + nb\sin(x)W_2 + \nu\beta'_x,$$

$$M_{x\theta} = (1-\nu)(-nb\beta'_x - nb^2\cos(x)W_3 + b\sin(x)W'_2 - b^2\sin(x)\cos(x)W_2),$$

$$V_x = Q_x + nbM_{x\theta}, \qquad S_{x\theta} = N_{x\theta} + b\sin(x)M_{x\theta}, \qquad \beta_x = W_1 - W'_3, \tag{25}$$

where $b = 1/(\sin(x) + R_0/R)$. The normalized non-zero elements of the coefficient matrix $[U(x)]$ of dimension eight are as follows (in these coefficients, $d+2$ is replaced with d since $d \gg 1$; this simplification improves the integration process of these coefficients tremendously, and it can be shown to have a negligible effect on the results):

$$U_{31} = U_{45} = U_{57} = -U_{34} = -U_{67} = 1, \qquad U_{77} = -b\cos(x),$$

$$U_{68} = 2nb^3\sin^2(x)/d + 2nb^2\sin(x)/d - nb, \qquad U_{11} = U_{44} = -\nu b\cos(x),$$

$$U_{22} = b\cos(x) + 2b^3\sin^2(x)\cos(x)/d, \qquad U_{75} = -U_{43} = n^2\nu b^2,$$

$$U_{23} = 2nb^3\sin(x)\cos(x)/d, \qquad U_{24} = 2nb^2\sin(x)/d,$$

$$U_{78} = -4nb^3\sin(x)\cos(x)/d, \qquad U_{21} = nb,$$

$$U_{51} = -2n^2b^3(1-\nu)\sin(x), \qquad U_{58} = -4nb^2\sin(x)/d,$$

$$U_{85} = -U_{42} = n\nu b^2\sin(x), \qquad U_{86} = -U_{12} = \nu nb,$$

$$U_{55} = U_{66} = -b(1-\nu)\cos(x), \qquad U_{28} = 2/d(1-\nu),$$

$$U_{76} = -U_{13} = 1 + \nu b \sin(x), \qquad U_{16} = 1/d,$$

$$U_{52} = nb^3(1-\nu^2)\sin(x)\cos(x) - 4nb^5(1-\nu)\sin^3(x)\cos(x)/d,$$

$$U_{88} = -2b\cos(x) - 2b^3\sin^2(x)\cos(x)(3\sin(x) - 1/b)/d,$$

$$U_{62} = ndb^2(1-\nu^2)\cos(x) + 2nb^6\sin^3(x)\cos(x)(\sin(x) + 1/b)/d,$$

$$U_{81} = ndb^2(1-\nu^2)\cos(x) - nb^4(1-\nu)\sin(x)\cos(x)(3\sin(x) - 1/b),$$

$$U_{54} = 2n^2b^2(1-\nu) + (1-\nu^2)\cos^2(x) - 4n^2b^4(1-\nu)\sin^2(x)/d,$$

$$U_{64} = -n^2b^3(1-\nu)(\sin(x) + 1/b) + 2n^2b^6(1-\nu)\sin^2(x)(\sin(x) + 1/b)/d,$$

$$U_{61} = n^2b^4(1-\nu)\sin(x)(\sin(x) + 1/b) + b^2(1-\nu^2)d\cos^2(x) - \lambda,$$

$$U_{53} = U_{74} = n^2b^3(1-\nu)(3+\nu)\cos(x) - 4n^2b^5(1-\nu)\sin^2(x)\cos(x)/d,$$

$$U_{71} = b^2(1-\nu^2)d\sin(x)\cos(x) - 2n^2b^4(1-\nu)\sin(x)\cos(x),$$

$$U_{72} = nb^2(1-\nu^2)d\sin(x) + n^3b^4(1-\nu^2)\sin(x) - 4nb^6(1-\nu)\sin^3(x)\cos^2(x)/d,$$

$$U_{82} = n^2b^2(1-\nu^2)d - 2b^4(1-\nu)\sin^2(x)\cos^2(x) + n^2b^4(1-\nu^2)\sin^2(x) - 2b^6(1-\nu)\sin^3(x)\cos^2(x)(3\sin(x) - 1/b)/d - \lambda,$$

$$U_{73} = n^4b^4(1-\nu^2) + 2n^2b^4(1-\nu)\cos^2(x) + b^2(1-\nu^2)d\sin^2(x) - 4n^2b^6(1-\nu)\sin^2(x)\cos^2(x)/d - \lambda,$$

$$U_{63} = b^2(1-\nu^2)d\sin(x)\cos(x) - n^2b^4(1-\nu)\cos(x)(\sin(x) + 1/b) + 2n^2b^5(1-\nu)\sin^2(x)\cos(x)(\sin(x) + 1/b)/d,$$

$$U_{83} = nb^2(1-\nu^2)d\sin(x) + n^3b^4(1-\nu^2)\sin(x) - 2nb^6(1-\nu)\sin^2(x)\cos^2(x)(3\sin(x) - 1/b)/d,$$

$$U_{84} = nb^3(1-\nu^2)\sin(x)\cos(x) + nb^3(1-\nu)\cos(x)(\sin(x) - 1/b) - 2nb^5(1-\nu)\sin^2(x)\cos(x)(3\sin(x) - 1/b)/d. \tag{26}$$

A quarter of a complete torus clamped at both edges is used here for comparison purposes. This segment is located 50·8 mm from the axis of symmetry ($R_0 = 50{\cdot}8$ mm), and has a 25·4 mm radius, a 2·03 mm thickness, and material properties $E = 207$ GPa, $\rho = 7800$ kg/m^3 and $\nu = 0{\cdot}3$. It is oriented such that $x_0 = 0°$ and $x_1 = 90°$. Since no published theoretical data on the toroidal shell could be found, SSM results are only compared with FEM results in Table 6. SSM results are based on a step size of $h = L/50$, while FEM results are based on a 20-element axisymmetric model.

TABLE 6

Clamped-clamped torus: comparison of natural frequencies in Hz

n	SSM	FEM [49]	Δ%
0	18 926	18 910	0·1
1	19 112	19 087	0·1
2	19 740	19 712	0·1
3	20 876	20 840	0·2

$\Delta\% = 100 \times (\text{SSM} - \text{FEM})/\text{SSM}$.

4. SYNTHESIS OF SHELL STRUCTURES

4.1. CYLINDER-CYLINDER COMBINATION

The objective here is to join s circular cylindrical shells as shown in Figure 6(a). With the exception of the common radius, all these cylinders may have different geometrical dimensions and material properties. Thes state vectors at the boundaries of the overall structure can be related to each other through the overall transfer matrix

$$[T(x_{0g}, x_{1g})] = [T(x_{0s}, x_{1s})][C]_{s-1}[T(x_{0s-1}, x_{1s-1})][C]_{s-2} \cdots [C]_1[T(x_{01}, x_{11})]. \quad (27)$$

Here, the first subscript indicates the boundary, while the second one identifies the substructure. The non-zero elements of the substructure coupling matrix $[C]_i$ are

$$C_{11} = C_{22} = C_{33} = C_{44} = 1, \qquad C_{55} = C_{66} = C_{77} = C_{88} = D_{i+1}/D_i, \qquad i = 1, 2, \ldots, s. \quad (28)$$

The case of inconsistent substructure co-ordinate systems is best demonstrated by considering joining the two cylinders shown in Figure 6(b). The overall transfer matrix for this case is given by

$$[T(x_{0g}, x_{1g})] = [G][T(x_{02}, x_{12})]^{-1}[G]^{-1}[C][T(x_{01}, x_{11})], \quad (29)$$

where the non-zero elements of $[C]$ are given in equations (28), $[G]^{-1} = [G]$, and the non-zero elements of $[G]$ are

$$G_{11} = G_{22} = -G_{33} = G_{44} = -G_{55} = -G_{66} = G_{77} = -G_{88} = -1. \quad (30)$$

As a specific example, the shear diaphragmed cylinder analyzed in section 3.1 is segmented into 2, 3 or 4 cylinders of equal thicknesses and material properties but different lengths. The segments are then joined together according to the procedure explained above. Since the resulting eigenvalues are identical to those given in Table 1, they are not repeated here. Also, no mode shapes are presented here due to their trivial nature.

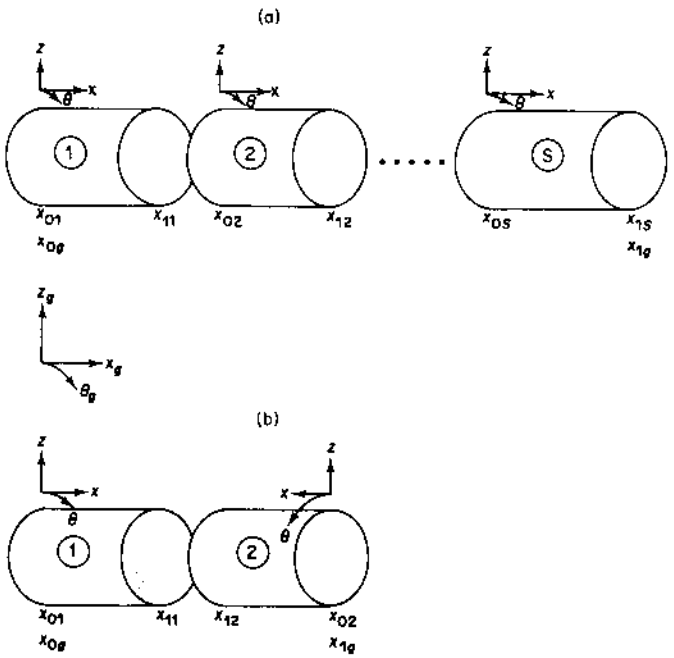

Figure 6. Cylinder-cylinder combination: (a) consistent co-ordinates; (b) inconsistent co-ordinates.

4.2. HEMISPHERE-HEMISPHERE COMBINATION

Figure 7 shows the cross-sectional view of two hemispheres to be joined. The overall transfer matrix for this case is

$$[T(x_{0g}, x_{1g})] = [T(x_{02}, x_{12})][C][T(x_{01}, x_{11})], \tag{31}$$

where the elements of $[C]$ are given by equations (28).

As discussed in section 3.3, there is a pinhole with free boundary conditions at the apex of each hemisphere:

$$x_{01} = 0{\cdot}1°, \qquad x_{11} = x_{02} = 90°, \qquad x_{12} = 179{\cdot}9°. \tag{32}$$

As a specific example, the full sphere presented in section 3.3 is broken into two identical hemispheres, and joined back together. The eigenvalues of the resulting full sphere are identical to those given in Table 5. A few modes of interest are presented in Figure 8 over a quarter sphere region. The lowest $n = 0$ mode has two nodal circles along x. The lowest $n = 2$ mode has no nodal circles along x, but it has two nodal circles along θ. Therefore, these two modes are essentially the same due to the spherical symmetry, and they have the same natural frequencies.

4.3. CONE-CYLINDER COMBINATION

Figure 9 shows the cross-sectional view of a circular cylinder clamped at one end and rigidly attached to a complete cone at the other end. The global transfer matrix $[T(x_{0g}, x_{1g})]$ is given by equation (31). Since the substructure co-ordinate systems are consistent with the global one, no co-ordinate adjustment is needed. The substructure coupling matrix $[C]$ for this case is

$$\begin{aligned} C_{22} = C_{44} = 1, \qquad & C_{55} = C_{88} = D_2/D_1, \\ C_{11} - C_{33} = \cos(\gamma), \qquad & C_{31} = -C_{13} = \sin(\gamma), \\ C_{67} = C_{77} = (D_2/D_1)\cos(\gamma), \qquad & C_{76} = -C_{67} = (D_2/D_1)\sin(\gamma). \end{aligned} \tag{33}$$

As mentioned in section 3.2, the cone is modeled as a truncated cone with a free pinhole at its apex ($x_0/x_1 = 0{\cdot}01$). This is considered to be a reasonably accurate model of the

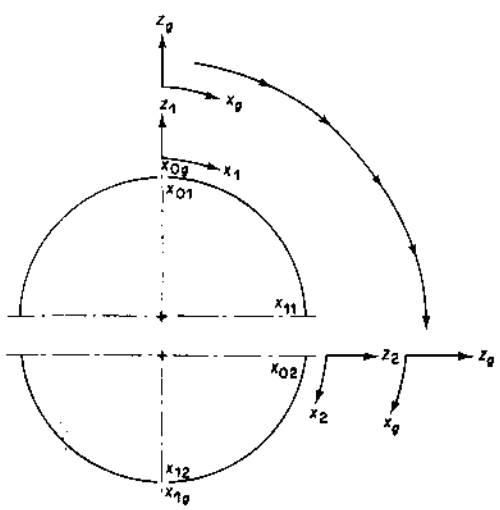

Figure 7. Hemisphere-hemisphere combination.

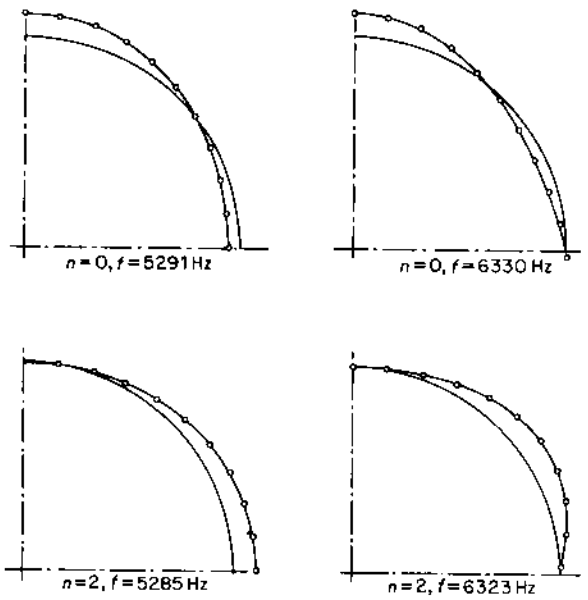

Figure 8. Mode shapes of the hemisphere-hemisphere combination.

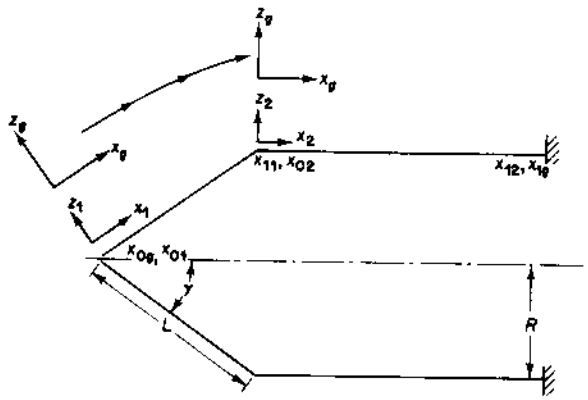

Figure 9. Cone-cylinder combination.

complete cone as far as the eigensolutions are concerned. However, it is inappropriate to use this model to predict force/moment information near the apex of a complete cone.

The procedure is applied to an example case for which the cone and the cylinder share a 114·3 mm radius, a 2·03 mm thickness, and the material properties $E = 207$ GPa, $\rho = 7800\ \text{kg/m}^3$ and $\nu = 0{\cdot}3$. The cylinder is 171·5 mm long, and the apex angle of the cone is $\gamma = 60°$. The results shown in Table 7 are based on a step size of $h = L/50$ for the cone, and an axisymmetric finite element model with 10 elements for the cone and 10 elements for the cylinder. SSM and FEM results are in close agreement for all modes.

The interaction between the cone and the cylinder is demonstrated by the mode shapes presented in Figure 10. There seems to be a low degree of interaction between the substructures for $n = 0$ and 1 modes. The degree of coupling increases for $n > 1$. Preservation of the 120° junction angle between the cone and the cylinder can be shown by increasing the resolution of these mode shapes.

TABLE 7

Cone-cylinder combination: comparison of natural frequencies in Hz

n	SSM	FEM [49]	Δ%
0	2525	2530	−0·2
	5585	5585	0·0
	6470	6478	−0·1
1	1962	1962	0·0
	3432	3435	−0·1
	5349	5354	−0·1
2	2087	2080	0·3
	3357	3358	0·0
	4618	4608	0·2
3	2117	2117	0·0
	2465	2465	0·0
	4570	4576	−0·1

$\Delta\% = 100 \times (\text{SSM} - \text{FEM})/\text{SSM}$.

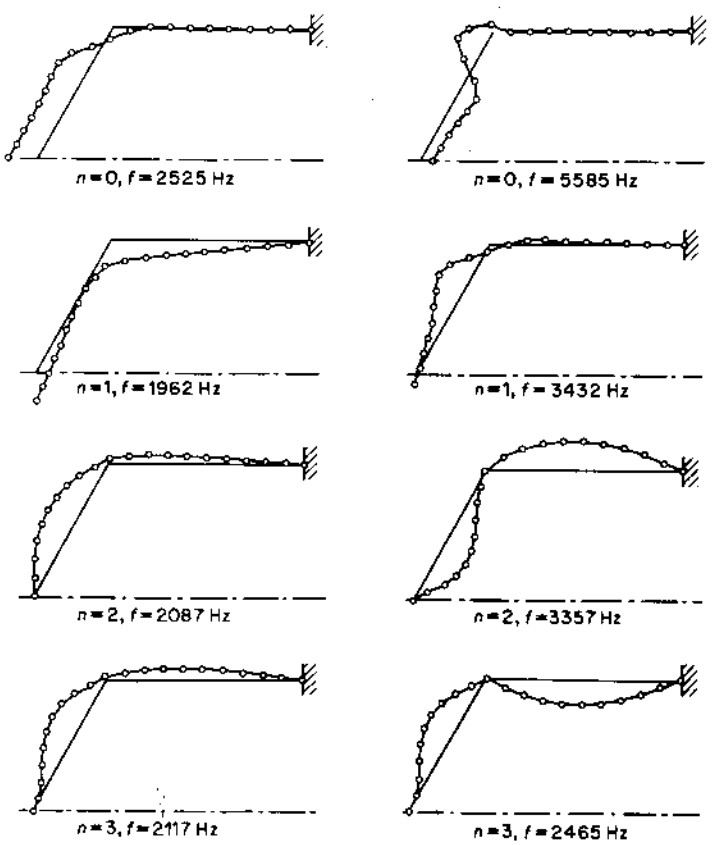

Figure 10. Mode shapes of the cone-cylinder combination (preservation of joint angles can be seen in higher resolution plots).

4.4. HERMETIC CAPSULE

A hermetic capsule which consists of a circular cylinder closed at both ends with hemispherical end caps is shown in Figure 11. The global transfer matrix for this case is given by

$$[T(x_{0g}, x_{1g})] = [T(x_{03}, x_{13})][C][T(x_{02}, x_{12})[C][T(x_{01}, x_{11})], \tag{34}$$

where

$$x_{01} = 0{\cdot}1^\circ, \qquad x_{11} = x_{03} = 90^\circ, \qquad x_{13} = 179{\cdot}9^\circ. \tag{35}$$

Here, the substructure coupling matrix $[C]$ for both end caps is given by equation (28), and no co-ordinate transformation is necessary because of the consistency between all of the co-ordinate systems. Free boundary state vectors $\{\Phi(x_{0g})\}$ and $\{\Phi(x_{1g})\}$ are enforced at the pinholes at the apices of the end caps. One can simplify the solution procedure for this case by taking advantage of the symmetry of this structure about A-A as shown in Figure 11. The transfer matrix for the half capsule is

$$[T(x_{0g}, x^*_{1g})] = [T(x_{01}, x_{11})][C][T(x_{02}, x^*_{12})]. \tag{36}$$

The symmetric and antisymmetric modes about A-A can be found by enforcing the boundary conditions:

$$\begin{aligned} \{\Phi(x^*_{1g})\}^{\mathrm{T}} &= \langle W_1, 0, 0, \beta_x, 0, 0, V_x, S_{x\theta}\rangle \qquad \text{for antisymmetric modes;} \\ \{\Phi(x^*_{1g})\}^{\mathrm{T}} &= \langle 0, W_2, W_3, 0, M_x, N_x, 0, 0\rangle \qquad \text{for symmetric modes.} \end{aligned} \tag{37}$$

The procedure is applied to a half capsule for which the hemisphere and the cylinder are 114·3 mm in radius, 2·03 mm in thickness, and have the material properties $E =$ 207 GPa, $\rho = 7800$ kg/m^3 and $\nu = 0{\cdot}3$. The cylinder is 171·5 mm long. The first three natural frequencies for a given circumferential mode number n are presented in Table 8. The agreement between SSM and FEM results is once again excellent. Some of the corresponding SSM mode shapes are also presented in Figure 12. Again, the cylinder seems to become the dominant vibrating substructure as the circumferential mode number increases. The end caps dominate the $n = 0$ mode.

4.5. REFRIGERATION COMPRESSOR SHELL

As an example of a relatively complex axisymmetric hermetic shell structure, a refrigeration compressor shell is modeled with SSM. The results are then compared with FEM predictions and measured data. Figure 13 shows the cross-sectional view of this axisymmetric structure which is made of steel ($E = 207$ GPa, $\rho = 7800$ kg/m^3 and $\nu = 0{\cdot}3$). While

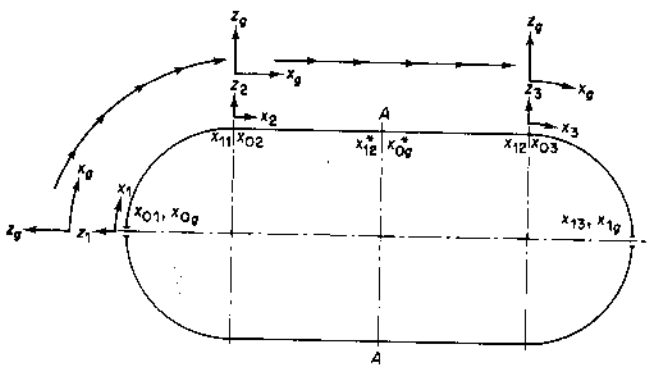

Figure 11. Hermetic capsule.

TABLE 8

Hermetic capsule: comparison of natural frequencies in Hz

	Symmetric modes			Antisymmetric modes		
n	SSM	FEM [49]	Δ%	SSM	FEM [49]	Δ%
0	4011	4005	0·1	5539	5538	0·0
	6292	6297	−0·1	6671	6666	0·1
	6812	6808	0·1	7016	7014	0·0
1	2740	2742	−0·1	4198	4201	−0·1
	5790	5797	−0·1	5086	5089	−0·1
	5933	5934	0·0	6335	6336	0·0
2	854	855	−0·1	2471	2476	−0·2
	3946	3955	−0·2	5015	5024	−0·2
	5712	5720	−0·1	6134	6138	−0·1
3	601	602	−0·2	1732	1732	−0·3
	3000	3009	−0·3	4099	4110	−0·3
	4954	4966	−0·2	5603	5617	−0·2

$\Delta\% = 100 \times (\text{SSM} - \text{FEM})/\text{SSM}$.

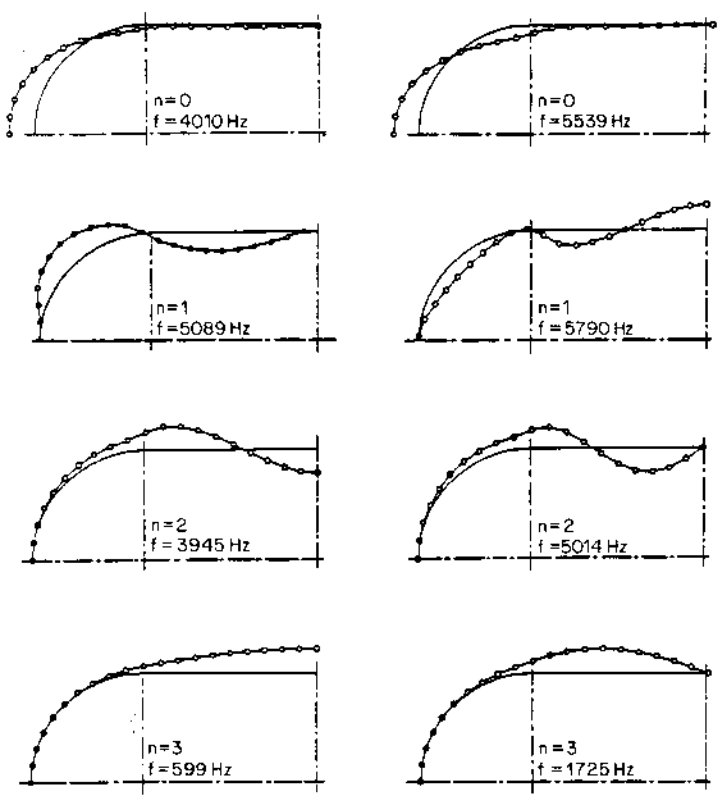

Figure 12. Mode shapes of the hermetic capsule.

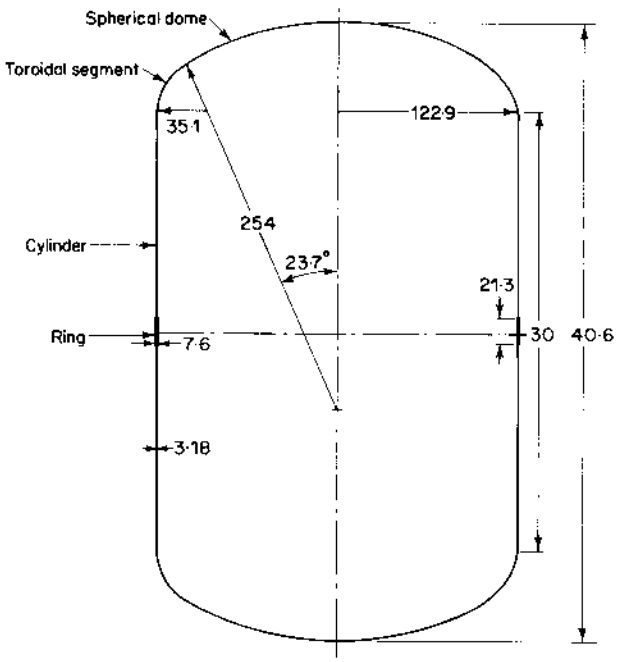

Figure 13. Cross-sectional view of a typical refrigeration compressor shell (all dimensions in mm).

various shell elements are identified in this figure, some of the local attachments (pipe, tube, valve, etc.) are not shown. The measured data were collected by exciting the structure (with air inside) with a shaker attached to the cylindrical body and fed with a random signal. Over the frequency range of 0–2000 Hz, 12 resonant frequencies were detected, which are given in Table 9. It was established that the first six frequencies represent only three circumferential modes as the well-known modal splitting phenomenon for nearly axisymmetric structures [58] was observed. The correlation between the natural modes and frequencies is also given in Table 9.

Natural frequencies identified as "bottom modes" correspond to modes which showed significant amplitudes in the bottom half of the compressor below the welded seam, and showed very little motion in the top half. Also, the end caps did not seem to have any significant vibrations for any of the resonances detected in this range. This was evident from the high signal-to-noise ratio obtained when the accelerometer was placed on the end caps.

In a fashion similar to the modeling of the hermetic bullet, the state space model of the compressor shell was constructed by the systematic assemblage of the appropriate shell elements selected from a prepared library of various shell geometries already discussed in section 3. A spherical dome was joined to a toroidal shell segment to form the end cap with dimensions shown in Figure 13. They were then joined to a cylinder 139·2 mm long and 3·2 mm thick representing half of the body of the compressor shell. This cylinder was joined to another cylinder 10·7 mm long and 7·6 mm thick representing half of the welded seam. The other half of the compressor shell could have been modeled similarly, but the computational task was made easier by analyzing only the half-model and enforcing the boundary conditions (37) at the mid-section of the shell. Similar to the case of the hermetic capsule, the initial boundary x_{0g} of the compressor shell model is a free pinhole at the apex of the end cap.

TABLE 9

Experimentally identified natural frequencies and mode shapes for compressor shell

f (Hz)	Mode (m, n)
867, 880	Mode (0, 3)
1090, 1106	Mode (0, 2)
1143, 1158	Mode (0, 4)
1551, 1558, 1649	Bottom modes
1765, 1838, 1888	$m = 1$ Modes

TABLE 10

Refrigeration compressor shell: comparison of natural frequencies in Hz

n	SSM	FEM [49]	Δ%
0	2529	2528	0·0
1	3132	3105	0·9
2	1236	1239	−0·2
3	964	966	−0·2
4	1220	1222	−0·2
5	1744	1743	0·1

$\Delta\% = 100 \times (\text{SSM} - \text{FEM})/\text{SSM}$.

SSM and FEM results for the lowest natural frequency corresponding to the first five circumferential mode numbers are presented in Table 10. The corresponding mode shapes are shown in Figure 14. The fact that modes $n = 0$ and 1 are predominantly end cap modes and occur at frequencies larger than 2000 Hz explains why no end cap natural frequencies were detected over the 0–2000 Hz frequency range in the experimental analysis. In Figure 15, SSM results are shown to set the same trend as the measured data.

5. CONCLUDING REMARKS

A structural synthesis method based on state space mathematics was proposed for the eigensolution of axisymmetric joined/hermetic thin shell structures. Chief strengths of the state space method (SSM) include distributed parameter modeling and complete matching of boundary variables. Guidelines governing joining substructures with consistent as well as inconsistent co-ordinate systems were developed. The inherent numerical limitations of the method were significantly reduced by adopting the Padé approximation technique for matrix exponentiation. Also, the solution procedure of SSM was unified between space-invariant and space-variant substructures through a spatial discretization

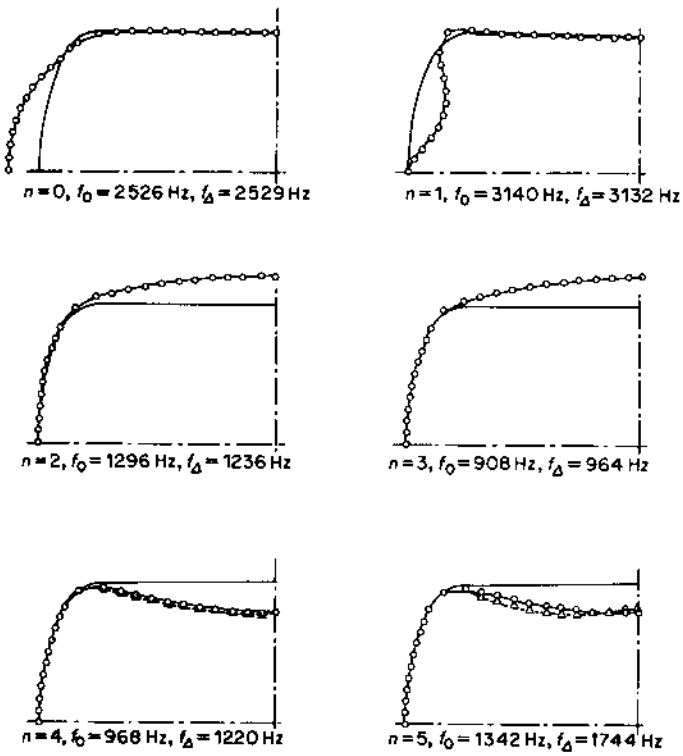

Figure 14. Mode shapes of the refrigeration compressor shell. △ · · · △, Welded; ○—○, no weld.

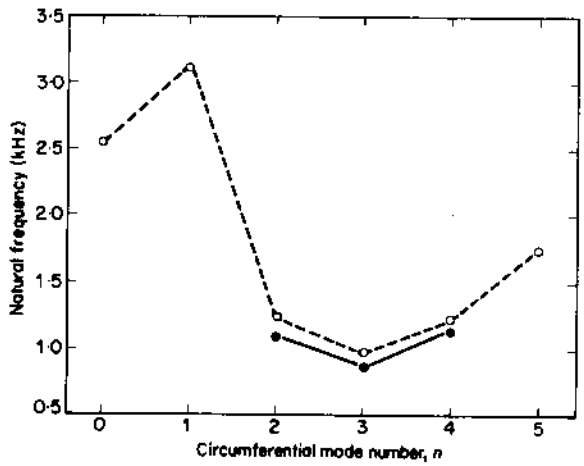

Figure 15. Comparison of SSM results with the measured data for the refrigeration compressor shell. —○—, SSM; —●—, experiment.

scheme. Validity of SSM was demonstrated through its application to cylindrical, conical, spherical and toroidal shells, and comparing the results with well-known theoretical solutions of these structural elements. The strength of SSM in structural synthesis was demonstrated through its application to various joined shell structures, including a hermetic capsule and a hermetic refrigeration compressor shell. In all cases SSM results

were supported by finite element method (FEM) predictions. In the case of the compressor shell, SSM compared well with the experiment, especially for natural frequency trends.

Despite the examples presented in this paper, SSM has yet to become as versatile as a general purpose structural synthesis method should be. One category of boundary conditions not currently incorporated in SSM belongs to a structure with more than two boundaries such as a rectangular plate which has two pairs of boundaries. Such a case was avoided in this work by limiting the scope to axisymmetric structures. Further work should include SSM modeling of multi-boundary geometries. Further, a comparative study concerning accuracy and efficiency is necessary before one can establish the computational advantages and/or disadvantages of SSM over other synthesis methods, especially FEM.

ACKNOWLEDGMENTS

The authors would like to thank Carlyle Compressor Company, Carrier Corporation, and especially Mr Thomas Katra for supporting this study. We are also indebted to ASHRAE for providing partial financial support.

REFERENCES

1. V. V. NOVOZHILOV 1964 *The Theory of Thin Elastic Shells.* Groningen, The Netherlands: Noordholf.
2. A. L. GOLDENVEIZER 1961 *Theory of Thin Shells.* New York: Pergamon Press.
3. W. FLUGGE 1962 *Stresses in Shells.* Berlin: Springer-Verlag.
4. H. KRAUS 1967 *Thin Elastic Shells.* New York: Wiley and Sons Inc.
5. A. E. H. LOVE 1944 *A Treatise on the Mathematical Theory of Elasticity.* New York: Dover.
6. A. W. LEISSA 1973 *NASA SP-288.* Vibration of shells.
7. W. SOEDEL 1981 *Vibrations of Shells and Plates.* New York: Dekker.
8. R. D. BLEVINS 1979 *Formulas for Natural Frequency and Mode Shape.* New York: Van Nostrand Reinhold.
9. R. N. ARNOLD and G. B. WARBURTON 1953 *Proceedings of Institution of Mechanical Engineers* **167**, 62–80. The flexural vibrations of thin cylinders.
10. E. B. BROOKBANK 1978 *Ph.D. Thesis, The Ohio State University.* Forced vibration of thin elastic shells with application to fractional horsepower hermetic refrigeration compressor shells.
11. L. L. FAULKNER and J. E. HAMILTON 1971 *Proceeding of International Congress on Refrigeration, Washington, D.C.* Refrigeration compressor shell vibration and sound radiation.
12. A. KALNINS 1964 *Journal of the Acoustical Society of America* **36**, 1355–1365. Free vibrations of rotationally symmetric shells.
13. W. C. L. HU and J. P. RANEY 1967 *AIAA Journal* **5**, 976–980. Experimental and analytical study of vibrations of joined shells.
14. B. L. SMITH and E. E. HAFT 1967 *AIAA Journal* **5**, 2080–2082. Vibrations of circular cylindrical shell closed by an elastic plate.
15. H. SAUNDERS and P. R. PASLAY 1959 *Journal of the Acoustical Society of America* **31**, 579–583. Inextensional vibrations of a sphere-cone shell combination.
16. I. U. OJALVO and M. NEWMAN 1967 *AIAA Journal* **5**, 1139–1146. Natural vibrations of a stiffened pressurized cylinder with an attached mass.
17. L. L. FAULKNER 1969 *Ph.D. Thesis, Purdue University.* Vibration analysis of shell structures using receptances.
18. Y. HIRANO 1969 *Bulletin of the Japan Society of Mechanical Engineers* **12**, 459–469. Axisymmetric vibrations of thin drums.
19. S. TAKAHASHI and Y. HIRANO 1970 *Bulletin of the Japan Society of Mechanical Engineers* **13**, 240–247. Vibration of a combination of circular plates and cylindrical shells (1st report: a cylindrical shell with circular plates at ends).

20. S. TAKAHASHI and Y. HIRANO 1971 *Bulletin of the Japan Society of Mechanical Engineers* **14**, 20–28. Vibration of a combination of circular plates and cylindrical shells (2nd report: a cylindrical shell with a circular plate in the intermediate section).
21. S. TAKAHASHI, Y. HIRANO and K. SUZUKI 1970 *Bulletin of the Japan Society of Mechanical Engineers* **13**, 850–857. Vibrations of a system connecting to cylindrical shells.
22. S. TAKAHASHI, K. SUZUKI, T. KOSAWADA and E. ANZAI 1981 *Bulletin of the Japan Society of Mechanical Engineers* **24**, 1826–1836. Vibrations of cylindrical shells with varying thickness.
23. S. TAKAHASHI, K. SUZUKI, E. ANZAI and T. KOSAWADA 1982 *Bulletin of the Japan Society of Mechanical Engineers* **25**, 1435–1442. Vibrations of conical shells with variable thickness.
24. S. TAKAHASHI, K. SUZUKI and T. KOSAWADA 1984 *Bulletin of the Japan Society of Mechanical Engineers* **27**, 786–793. Vibration of shell of revolution (improved theory).
25. S. TAKAHASHI, K. SUZUKI and T. KOSAWADA 1985 *Bulletin of the Japan Society of Mechanical Engineers* **28**, 117–123. Vibrations of conical shells with variable thickness (continued).
26. K. SUZUKI, E. ANZAI and S. TAKAHASHI 1982 *Bulletin of the Japan Society of Mechanical Engineers* **25**, 1108–1119. Vibrations of cylindrical shells with varying thickness (continued).
27. K. SUZUKI, M. KONNO, T. KOSOWADA and S. TAKAHASHI 1982 *Bulletin of the Japan Society of Mechanical Engineers* **25**, 1591–1600. Axisymmetric vibrations of a vessel with variable thickness.
28. K. SUZUKI, S. TAKAHASHI, E. ANZAI and T. KOSOWADA 1983 *Bulletin of the Japan Society of Mechanical Engineers* **26**, 1775–1782. Vibrations of a cylindrical shell with variable thickness capped by a circular plate.
29. K. SUZUKI, K. KIKUCHI, T. KOSOWADA and S. TAKAHASHI 1984 *Bulletin of the Japan Society of Mechanical Engineers* **27**, 974–979. Axisymmetric vibrations of thin shells of revolution.
30. T. KOSOWADA, K. SUZUKI and S. TAKAHASHI 1983 *Bulletin of the Japan Society of Mechanical Engineers* **26**, 2165–2171. Asymmetric vibrations of thin shells of revolution.
31. T. KOSOWADA, K. SUZUKI and S. TAKAHASHI 1984 *Bulletin of the Japan Society of Mechanical Engineers* **27**, 1983–1979. Vibrations of a combined system of circular plates and a shell of revolution.
32. W. C. HURTY 1960 *Proceedings of American Society of Civil Engineers* **86** (EM4), 51–69. Vibrations of structural systems by component mode synthesis.
33. W. C. HURTY 1965 *AIAA Journal* **3**, 678–685. Dynamic analysis of structural systems using component modes.
34. G. M. L. GLADWELL 1964 *Journal of Sound and Vibration* **1**, 41–59. Branch mode analysis of vibrating systems.
35. R. R. GRAIG and M. C. C. BAMPTON 1968 *AIAA Journal* **6**, 1313–1319. Coupling of substructures for dynamic analysis.
36. W. A. BENFIELD and R. HRUDA 1971 *AIAA Journal* **9**, 1255–1261. Vibration analysis of structures by component mode synthesis.
37. E. H. DOWELL 1972 *Journal of Applied Mechanics* **39**, 727–732. Free vibrations of an arbitrary structure in terms of component modes.
38. A. L. HALE and L. MEIROVITCH 1982 *Journal of Sound and Vibration* **84**, 269–287. A general procedure for improving substructures representation in dynamic synthesis.
39. S. HOU 1969 *Shock and Vibration Bulletin* **40**, 25–39. Review of modal synthesis techniques and a new approach.
40. T. IRIE, G. YAMADA and Y. KANEKO 1982 *Journal of Sound and Vibration* **82**, 83–94. Free vibration of a conical shell with variable thickness.
41. T. IRIE, G. YAMADA and Y. MURAMOTO 1984 *Journal of Sound and Vibration* **95**, 31–39. Free vibration of joined conical-cylindrical shells.
42. T. IRIE, G. YAMADA and T. TANAKA 1984 *Journal of Sound and Vibration* **95**, 249–259. Free vibration of a circular cylindrical double-shell system interconnected by several springs.
43. G. YAMADA, T. IRIE and Y. TAGAWA 1984 *Journal of Sound and Vibration* **95**, 117–126. Free vibration of non-circular cylindrical shells with variable circumferential profile.
44. G. YAMADA, T. IRIE and T. TAMIYU 1986 *Journal of Sound and Vibration* **108**, 294–304. Free vibration of circular cylindrical double-shell system closed by end plates.
45. T. IRIE, G. YAMADA and Y. KOBAYASHI 1984 *Journal of Sound and Vibration* **96**, 133–142. Free vibration of a non-circular cylindrical shells with longitudinal interior partitions.
46. T. IRIE, G. YAMADA and H. IDA 1985 *Journal of Sound and Vibration* **102**, 229–241. Free vibration of longitudinally stiffened prismatic shells with and without partitions.

47. Y. KOBAYASHI and T. IRIE 1987 *Journal of the Acoustical Society of America* **81**, 1795–1800. Free vibration of unsymmetrically joined shell structures with a closed member.
48. D. M. TRUJILLO 1975 *International Journal for Numerical Methods in Engineering* **9**, 259–270. The direct numerical integration of linear matrix differential equations using Padé approximation.
49. *ANAYS Engineering Analysis Systems User's Manual.* Pennsylvania: Swanson Analysis Systems Inc.
50. E. C. PESTEL and F. A. LECKIE 1963 *Matrix Methods in Elastomechanics.* New York: McGraw-Hill.
51. S. SESHADRI 1977 *Sound and Vibration Bulletin* **47**, 121–133. Extended transfer matrix method for free vibration of shells of revolution.
52. C. MOLER and C. VAN LOAN 1978 *SIAM Review* **20**, 801–837. Nineteen dubious ways to compute the exponential of a matrix.
53. *CTRL-C User's Guide.* California: Systems Control Technology Inc.
54. L. A. PIPES 1963. *Matrix Methods for Engineering.* Englewood Cliffs, New Jersey: Prentice-Hall.
55. E. C. NAUMANN 1968 *NASA TN D-4772.* On the prediction of the vibratory behavior of free-free truncated conical shells.
56. H. M. ADELMAN, D. S. CATHERINES and W. C. WALTON 1969 *NASA TN D-4972.* A method for computation of vibration modes and frequencies of orthotropic thin shells of revolution having general meridonial curvature.
57. A. SILBIGER 1962 *Journal of the Acoustical Society of America* **34**, 862. Nonaxisymmetric modes of vibration of thin spherical shells.
58. W. SOEDEL 1980 *Proceedings of Purdue Compressor Technology Conference*, 259–262. Simple mathematical models of mode splitting of hermetic compressor shells that deviate from axisymmetry.

APPENDIX: NOMENCLATURE

A	cross-sectional area
$[C]$	substructure coupling matrix
D	bending stiffness, $= EH^3/12(1-\nu^2)$
d	$= 12R^2/H^2$
E	Young's modulus of elasticity
EXP	experiment
FEM	finite element method using reference [49]
f	natural frequency in Hz
$[G]$	co-ordinate transformation matrix
H	thickness
h	numerical discretization step size for space-variant substructures
I	cross-sectional area moment of inertia
L	normalized substructure length between boundaries x_0 and x_1
m	axial mode index indicating the number of nodal points along x excluding boundaries
$\underline{M}_x$	bending moment at x boundary
M_x	normalized bending moment at x boundary
$\underline{M}_\theta$	bending moment at θ boundary
M_θ	normalized bending moment at θ boundary
$\underline{M}_{x\theta}$	twisting moment at x boundary
$M_{x\theta}$	normalized force along x at x boundary
$\underline{N}_x$	force along x at x boundary
N_x	normalized force along x at x boundary
$\underline{N}_\theta$	force along θ at θ boundary
N_θ	normalized force along θ at θ boundary
$\underline{N}_{x\theta}$	in-plane shear force at x boundary
$N_{x\theta}$	normalized in-plane shear force at x boundary
n	circumferential mode index indicating the number of sine waves around the circumference
Q_x	transverse shear force at x boundary
$\bar{Q}_x$	normalized transverse shear force at x boundary

Q_θ	transverse shear force at θ boundary
$\bar{Q}_\theta$	normalized transverse shear force at θ boundary
R	radius
$S_{x\theta}$	in-plane Kirchhoff shear force at x boundary
$\bar{S}_{x\theta}$	normalized in-plane Kirchhoff shear force at x boundary
SSM	state space method
$T[(x_0, x)]$	transfer matrix relating state vectors at x_0 and x
$[U]$	normalized substructure coefficient matrix
V_x	transverse Kirchhoff shear force at x boundary
$\bar{V}_x$	normalized transverse Kirchhoff shear force at x boundary
W_1	displacement along x
$\bar{W}_1$	normalized displacement along x
W_2	displacement along θ
$\bar{W}_2$	normalized displacement along θ
W_3	transverse displacement along z
$\bar{W}_3$	normalized transverse displacement along z
x	substructure co-ordinate spanning from boundary to boundary
$\bar{x}$	normalized substructure co-ordinate spanning from boundary to boundary
x_g	normalized global co-ordinate spanning from boundary to boundary
x_{0i}, x_{1i}	normalized boundary co-ordinates of substructure i
x_{0g}, x_{1g}	normalized global boundary co-ordinates
z	normalized substructure co-ordinate normal to the surface
z_g	normalized global co-ordinate normal to the surface
α	$\rho AL^4\omega^2/EI$
β_x	slope along x
$\bar{\beta}_x$	normalized slope along x
θ	substructure circumferential co-ordinate
θ_g	global circumferential co-ordinate
λ	$\rho HR^4\omega^2/D$
ν	Poisson ratio
ρ	mass density
$\{\Phi(x)\}$	spatial state vector at x boundary
ω	circular frequency in rad/s
$(\ )'$	$\mathrm{d}(\ )/\mathrm{d}x$
$\{\ \}^T$	vector transpose
$[\ ]^{-1}$	matrix inverse